Damage Detection and Material Property Reconstruction of Composite Laminates Using Laser Ultrasonic Technique

QIU Jinhao[1,2*], *TAO Chongcong*[1,2], *JI Hongli*[1,2], *ZHANG Chao*[1,2], *ZHAO Jinling*[1,2,3]

1. State Key Laboratory of Mechanics and Control of Mechanical Structures, Nanjing University of Aeronautics and Astronautics, Nanjing 210016, P.R. China;

2. College of Aerospace Engineering, Nanjing University of Aeronautics and Astronautics, Nanjing 210016, P.R. China;

3. School of Mechanical and Power Engineering, Nanjing Tech University, Nanjing 211800, P.R. China

(Received 14 December 2018; revised 28 December 2018; accepted 5 January 2019)

Abstract: Laser ultrasonic technique has received increasing attentions in the past decade due to its contactless nature and a wide range of applications have been reported. In this review, applications of laser ultrasonic technique developed at Nanjing University of Aeronautics and Astronautics (NUAA) as well as elsewhere for non-destructive testing in composite laminates are presented. The principles of generating and detecting in a laser ultrasonic system are introduced, three different system configurations are also introduced with each configuration's advantages and disadvantages explained. More importantly, two major applications developed at NUAA for composite laminates are presented including damage detection, stiffness reconstruction and fatigue life prediction. Both applications are realized by a fixed-point PZT sensor and scanning pulse laser based on the linear reciprocal theorem. Analytical method and numerical models are employed and developed to realize the functionalities.

Key words: laser ultrasonic; composite laminates; damage detection; stiffness reconstruction

CLC number: V258 **Document code**: A **Article ID**: 1005-1120(2019)01-0001-16

0 Introduction

Fiber reinforced polymers (FRP) are widely used in engineering applications recently due to their superior mechanical properties over traditional metallic materials such as damage tolerance, fatigue and corrosion resistance and especially their high specific stiffness and strength. However, traditional composite structures e.g. composite laminates also come with their weaknesses such as sensitivity to impact damages, non-critical damage developments under relative low loads and composite laminates also show decrease in load-bearing capacity when subjected to cyclic loads. Therefore, various non-destructive testing (NDT) methods have been proposed and tested for damage detections in composite laminates, among which, laser ultrasonic technique shows great potentials due to its contactless nature.

Ultrasonic is a widely used approach for damage detection, the most traditional one being ultrasonic C-scan[1]. One or more probes are usually used to generate and sense bulk ultrasonic waves, which propagate in the structure in the thickness direction as shown in Fig.1(a). The collected data of transmitted and reflected waves are processed in the time domain or frequency domain to detect the internal damages in structures. However, the detection result, which depends on the experience and skill of inspectors, suffers from the complex interference of multiple reflected and diffracted waves in thin plate-like structure. In addition, direct-contact scan and indirect-contact scan through the media (such as water and oil) are costly and labor intensive, especially in large-scale inspection applications.

Apart from ultrasonic C-scan approach, the

*Corresponding author, E-mail address: qiu@nuaa.edu.cn.

How to cite this article: QIU Jinhao, TAO Chongcong, JI Hongli, et al. Damage Detection and Material Property Reconstruction of Composite Laminates Using Laser Ultrasonic Technique[J]. Transactions of Nanjing University of Aeronautics and Astronautics, 2019,36(1):1-16.

http://dx.doi.org/10.16356/j.1005-1120.2019.01.001

Lamb wave-based NDE techniques that have been widely used in plate-like structures also show appealing features in detecting damages because Lamb wave has the advantages of high sensitivity to various damage types and the capability of long transmission distance[2-3]. And in general, Lamb wave can be generated and received by piezoelectric sensor pairs[4] that are distributed over the inspection region, as shown in Fig.1(b). By analyzing the changes of Lamb wave propagation characteristics or using the time-of-flight information of the scattered waves, the damage position can be detected. However, contact-type transducers that are usually surface mounted or embedded on the test structures lead to some limitations of this method in wide applications that: (1) the excitation and sensing positions are fixed at several discrete points. To improve the inspection quality and extend the inspection region, a large amount of piezoelectric sensors are required; (2) transducer installation and cabling can be costly and labor intensive, especially in the large-scale inspection applications; (3) many contact transducers are not applicable under harsh environments such as high temperature and radioactive conditions; and (4) the added weight of the transducers and cables is not cost-effective in practical applications.

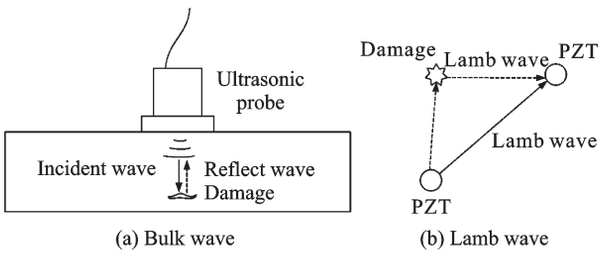

Fig. 1 Different inspection principles using bulk and lamb waves

Laser ultrasonic technique uses pulse laser to generate ultrasonic waves and overcomes most of the aforementioned disadvantages. The generation of ultrasound with lasers can actually go back to nearly as far as the invention of the first ruby laser, which was used to generate ultrasound or shock waves in materials[5-6]. Ultrasonic can be excited by laser through two different approaches: a thermoelastic way or a vaporized way, the former is truely non-destructive while the latter can cause surface damages. Since the scope of this review is focused on applications in NDT fields, only the thermoelastic approach will be included. The principle of ultrasonic excitation based on thermoelastic mechanism is to heat the material locally to expand, thereby producing a strain and a corresponding stress that becomes the source of wave propagating[7]. The heated point inside the material is a center of expansion to which 3 orthogonal force dipoles can be associated[8-9], thus the material effectively becomes the emitting transducer of ultrasound. Besides emitting transducer[10-13], laser can also be used as receiving transducer with an interferometer, which results in three different configurations for a laser ultrasonic system: fixed-point PZT sensor with scanning pulse laser, fixed-point PZT excitation with scanning laser Doppler vibrometer (LDV) sensing and pulse laser excitation with LDV sensing, the first two being a semi-laser system and the third a true laser system. Brief descriptions of the three systems are as follows.

Strategy 1 Fixed-point PZT sensor and scanning pulse laser—The system of the first scheme in Fig.2 consists of a Q-switched diode-pumped solid-state laser, a galvanometric laser mirror scanner, an acoustic emission (AE) sensor, a programmable filter, a digitizer, and a computer for hardware control and image processing. A schematic diagram of the entire experimental system configuration is shown in Fig.3. The AE sensor providing ultrasonic reception is fixed and focuses at a particular sensing region on the

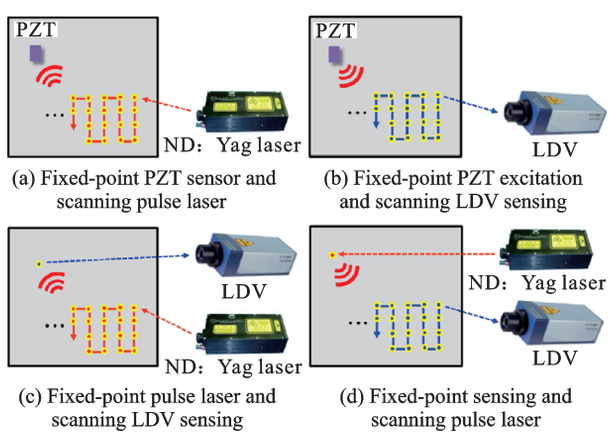

Fig. 2 Four different laser scanning schemes for wavefield visualization[14]

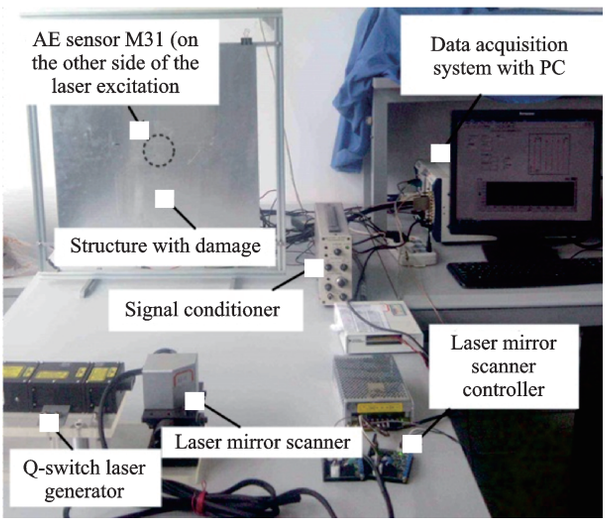

Fig.3 Experimental setup

specimen, whereas the laser beam acting as ultrasonic generation is directed to the targeted specimen with the help of a laser mirror scanner for remote and controllable scanning of the targeted area. The filters, digitizer, and computer hardware are used for data acquisition and image processing for damage evaluation and visualization. All devices are packed in a controller.

During the data acquisition process, the different ultrasonic responses between movable ultrasonic source point A and fixed sensor point B can be obtained experimentally as Case 1 in Fig.4. Based on the linear reciprocal theorem[15-16] the wave propagation from point A to B can be directly converted into the propagation from point B to A. Thus, the obtained data in Case 1 can represent the wave propagation from the fixed laser point B to an inspection region, which is distributed with a series of AE sensors as shown in Case 2 from Fig.4. Then, the responses of each scanning point at the same time t are plotted on an intensity snapshot to represent the wavefield at time point t. Finally, the snapshots are continually displayed in a time series and show the wave propagation in the inspection region as shown in Fig.5[17].

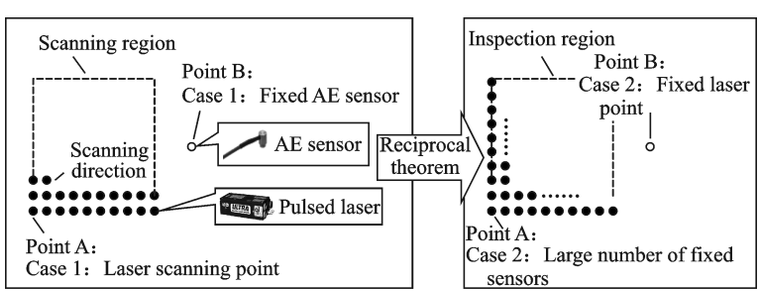

Fig.4 Schematic diagram of laser ultrasonic scanning technique

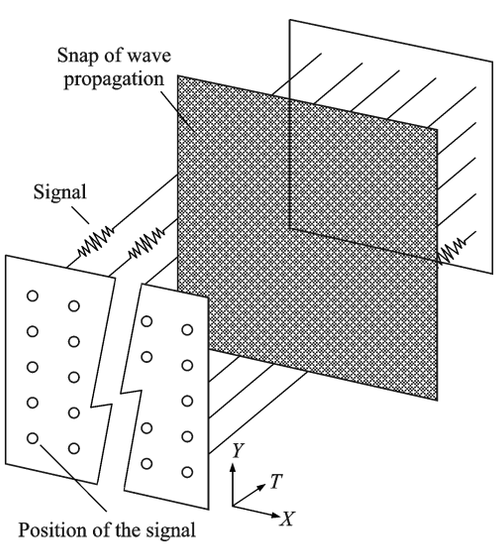

Fig.5 Data structure in wave propagation visualization

Strategy 2 Fixed-point PZT excitation and scanning LDV sensing—Different from Strategy 1, the data acquisition from this inspection strategy can be directly regarded as the Case 2 in Fig.4. The waveform generated by the piezoelectric transducer can be controlled by the input signal, which is more flexible in inspection application. When the sensing laser beam is perpendicular to the polished target surface, the signal to noise ratio (SNR) of the ultrasonic signal is high due to the majority of the incident laser beam being reflected straight back to the receiver. However, the SNR of the ultrasonic decreases as the incident angle of the laser beam increases. Thus, multiple ultrasonic signals often need to be measured at a single sensing point and averaged to improve the SNR[18].

Strategy 3 LDV sensing and pulse laser exci-

tation—When fixing the LDV sensing point and scanning the pulse laser in the inspection region, the ultrasonic propagation can be constructed sharing the same principle with Strategy 1. On the contrary, the situation that is to scan the LDV sensing point and fix the pulse laser is the same with Strategy 2. Both of them can achieve a complete noncontact inspection.

1 Damage Visualization Based on Laser Ultrasonic Imaging

A major application and advantage for laser ultrasonic in the field of NDT is the capability to achieve damage detection and visualization for both metallic and composite materials[19-31]. Lee et al. [20] proposed an ultrasonic propagation imaging for automatic damage visualization for steel pipeline with multiple kinds of damages in nuclear power plant. In their later work, Lee et al. [22]designed a laser ultrasonic system with functions of excitation, sensing, and diagnosis for damage visualization of target located at a long distance. A fixed-point PZT sensor and scanning pulse laser configuration was used. Sohn et al. [23]studied the applicability of non-contact wavefield imaging techniques to detect delamination and debond in composite structures, where a fixed-point PZT excitation and scanning LDV sensing configuration was used. Martarelli et al.[26] explored the applicability of delamination detection with laser ultrasonic. Chia et al.[24] emended PZT sensors into aircraft's wing structure made of CFRP material and utilized scanning laser to achieve visualization of damages and manufacture defects. An et al. [14] developed a complete noncontact laser ultrasonic scanning system with an LDV sensing and pulse laser excitation configuration, the system was applied for crack visualization and diagnosis in an aluminum plate. Liu et al. [30] also successfully located the fatigue crack in an aluminum plate using laser ultrasonic. In a more recent work, Park et al. [27] applied the noncontact laser ultrasonic system to detect delamination and debond in both a CFRP composite aircraft wing structure and a GFRP composite wind blade structure. Laser ultrasonic can also be used with other non-contact techniques to form a hybrid non-contact inspection system. Cavuto et al.[29] combined laser ultrasonic and air-coupled probe to improve the performance of train axle inspection. Dixon et al. [21] used laser ultrasonic in conjunction with electromagnetic acoustic transducer (EMAT) to detect cracks in metal sheets. In terms of real-world applications, Lee et al. [25]used optical fiber to direct the laser in a pipeline system for nuclear power plants to detect typical pipe defects without baseline data. Bate et al. [31] measured the texture in metal at elevated temperature using laser ultrasonic. Sun and Zhou [28] used laser ultrasonic to detect drill-induced delamination.

In the following, a damage visualization algorithm based on anomalous incident wave (AIW) developed at NUAA will be introduced to help readers better understand the principles of laser ultrasonic-based damage visualization.

1.1 Ultrasonic wave in damaged region

Assuming that the ultrasonic wave passes through a damage as shown in Fig.6. The incident wave $w_i(x,t)$ propagates along the positive x-direction and the reflected wave $w_r(x,t)$ propagates along the negative x-direction. Generally, the harmonic wave can be given by the following equations[14]

$$\begin{cases} w_i(x,t)=A\cos(\omega t-kx) & x\leqslant x_0-\dfrac{l_0}{2} \\ w_i(x,t)=B\cos(\omega t-kx+\alpha) & x>x_0+\dfrac{l_0}{2} \end{cases} \tag{1}$$

$$\begin{cases} w_r(x,t)=C\cos(\omega t+kx+\beta) & x\leqslant x_0-\dfrac{l_0}{2} \\ w_r(x,t)=0 & x>x_0+\dfrac{l_0}{2} \end{cases} \tag{2}$$

where ω is the angular frequency, k is the wavenum-

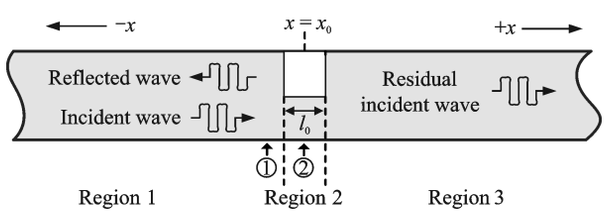

Fig.6 Schematic diagram of the ultrasonic wave interacting with a damage

ber, x_0 and l_0 represent the position and width of the slit, α and β are the phase shifts caused by the damage, A represents the incident wave amplitude while B and C represent the amplitudes of residual incident wave by transmission and reflected wave.

1.2 Damage detection algorithm using AIW energy map

To represent the discontinuous characteristic of the incident wavefield in the damage area, the AIW is defined as the differences between two incident wave signals obtained at adjacent points. Taking two incident wave signals $w_i(x,i)$ and $w_i(x+\Delta x, i)$ as an example, the AIW at the position x can be calculated as

$$\Delta w_i(x,i)=w_i(x,i)-w_i(x+\Delta x,i+d_{r\max}) \tag{3}$$

where Δx is the minimum spatial resolution of the laser scanning process and the time-lag $d_{r\max}$ can be calculated through a cross-correlation $r(d)$.

$$r(d)=\sum_{i=0}^{N} w_i(x,i)w_i(x+\Delta x,i+d) \tag{4}$$

where $d_{r\max}$ represents the time that the incident wave travels from x to $x+\Delta x$ to make $r(d_{r\max})$ reach the maximum value. Considering that the incident wave propagates in the continuous medium, two incident waves at the adjacent points are similar with each other. By using Eq.(3), the traveling incident wave in regions 1 and 3 as shown in Fig.6 can be eliminated. As a result, the energy changes in region 2 caused by the damage will be highlighted and the discontinuous characteristic of Eq.(1) is extracted. To evaluate the size and shape of the damage by a digital image, the AIW energy E_{AIW} can be calculated by the sum of squared AIW[32]

$$E_{\mathrm{AIW}}(x)=\sum_{i=1}^{N}\Delta w_i^2(x,i) \tag{5}$$

Compared with calculating anomalous wave directly from the original wavefield[17,33], the AIW extracts the wave propagation changes caused by the damage as well. However, due to the fact that the incident wave is much stronger than reflected wave in terms of signal strength, $d_{r\max}$ only denotes the time delay of the incident waves. Because the reflected wave and incident wave have the opposite time delays between the adjacent points, the reflected wave is also enlarged by this process. As the reflected wave propagating towards the health area in region 1, the energy of the anomalous wave is also distributed near the damaged area, which reduces the resolution of the damage image. After filtering the reflected wave, the AIW energy eliminates the reflected wave energy in health area that makes the shape of the damage much clearer.

As shown in Fig.6, a part of the incident wave is reflected with the propagation direction reversed. Because the damage is nonpenetrated, the other part of the incident wave passes through the damage and propagates in the original direction. Thus, the one-dimensional wave field $w(x,t)$ near the damage area can be given by combining the incident wave field $w_i(x,t)$ and reflected wave field $w_r(x,t)$.

$$w(x,t)=w_i(x,t)+w_r(x,t) \tag{6}$$

To construct the AIW map, the incident wave field w_i should be extracted from the original wave field w. From Eqs.(1,2), the major difference between the incident and reflected waves is the sign in front of the wavenumber k that indicates the wave propagation direction. To obtain the incident wave, two-dimensional Fourier transform (2D-FT) converts the wavefield from space-time (x-t) domain into wavenumber-frequency (k-ω) domain to separate the waves with different propagation directions as[34-35]

$$W(k,\omega)=\int_{-\infty}^{+\infty}\int_{-\infty}^{+\infty} w(x,t)\mathrm{e}^{-\mathrm{j}(kx+\omega t)}\mathrm{d}x\mathrm{d}t \tag{7}$$

where $W(k,\omega)$ is the wavefield in wavenumber-frequency domain and "j" represents the imaginary unit. The wavefield is divided into two parts: (1) the incident wave part that is in the quadrant with $k\omega<0$ and (2) the reflected wave part that is in the quadrant with $k\omega>0$. Two-dimensional inverse Fourier transform can then be applied to recover the time domain signals of these two components as follows

$$w_{i(r)}(x,t)=\frac{1}{2\pi}\int_{-\infty}^{+\infty}\int_{-\infty}^{+\infty} W(k,\omega)\Phi_{I(R)}\mathrm{e}^{-\mathrm{j}(kx+\omega t)}\mathrm{d}k\mathrm{d}\omega \tag{8}$$

where $\Phi_{I(R)}$ is a window function defined as follows, used to separate the incident and reflected waves.

$$\Phi_{I,R}=\begin{cases}0 & k\omega \geqslant 0\\ 1 & k\omega < 0\end{cases} \tag{9}$$

The principle is explained using 1D wave-field based 2D-FT as above. Similarly, the above 1D wave decomposition method can be extended to 2D case by means of 3D Fourier transform (3D-FT) and three-dimensional inverse Fourier transform (3D-IFT), for obtaining the wavefield by a laser ultrasonic scanning technique. Because the sensor response is collected by digital acquisition, the wavefield takes the form of discrete data. Thus, the Fourier transform can be realized by fast Fourier transform (FFT).

1.3 Experimental validation

To examine the feasibility of the proposed laser ultrasonic scanning system and image processing technique, the scheme using fixed-point AE sensor and scanning pulse laser as shown in Fig. 2 is employed for ultrasonic imaging and damage evaluation. Experiments of a composite structure were conducted.

A symmetric CFRP laminated plate with a stacking configuration of $[45°/-45°/0°/90°]_s$ is used to validate the damage evaluation method[32]. The in-plane dimensions of the CFRP plate are 480 mm×480 mm and the thickness is 1 mm. To make an artificial damage, a drop-weight impact test was performed according to Test Method D7136[36]. Damage is imparted through out-of-plane, concentrated impact (perpendicular to the plane of the CFRP plate) using a drop weight with a hemispherical striker tip as shown in Fig.7. The impact energy E_{impact} can be calculated by

$$E_{\text{impact}}=mgh \tag{10}$$

where m is the mass of the drop weight, g is the acceleration due to gravity and h is the drop-height. In this validation, the impact energy wasset to be 10 J and the impact damage cannot be detected visually. However, delamination, split and crack should exist inside the structure.

As shown in Fig. 8, the impacted side of the CFRP laminated plate is scanned by the movable laser point and the inspection region is 100 mm × 100 mm. The AE sensor is placed on the opposite

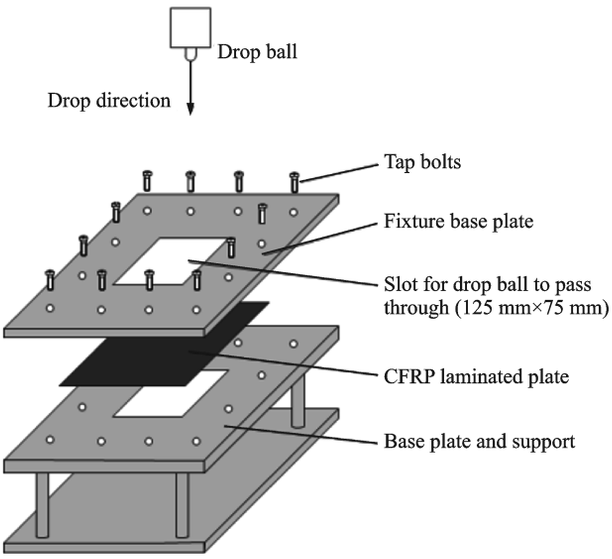

Fig.7 Schematic diagram of the drop-weight impact test for a CFRP plate

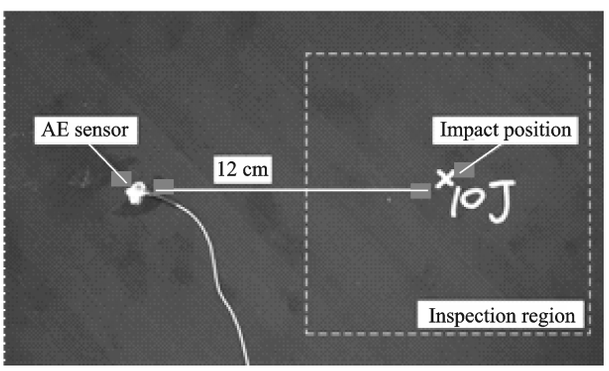

Fig.8 Picture of the CFRP plate with a damage caused by a 10 J impact

side of the CFRP plate with a distance of 12 cm away from the centre of the inspection region. The spatial interval of the laser scan is 1 mm and the signal is filtered with a band-pass frequency from 100 kHz to 200 kHz.

Two wavefields at the different time points are shown in Fig.9. Compared with the ultrasonic wave in a metal structure, the ultrasonic wave in the CFRP plate has low SNR due to the large material damping and the wave velocity is also lower. In order to ensure both of the S_0 and A_0 waves can pass through the inspection region, the sampling period is set to 200 μs. Same with the phenomenon in a metal plate with a slit, the amplitude changes around the damage region which can be used to detect the position of the damage.

The original wave energy map is constructed as

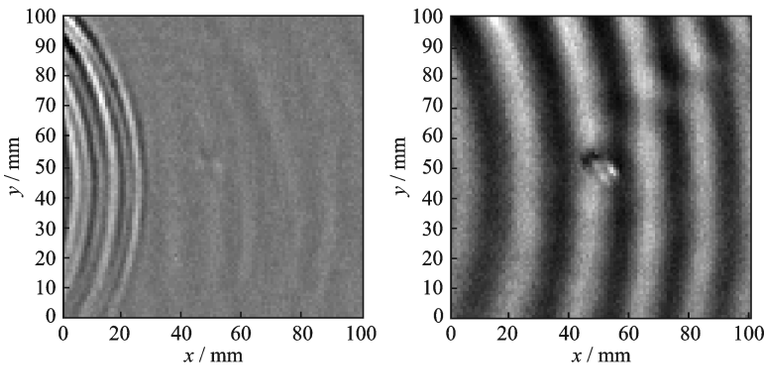

Fig. 9 Experimental wavefields at different times

shown in Fig.10. The wave energy decreases as the wave propagates. The anomalous wave energy region hardly shows the impact damage. To evaluate the inspection result, Fig.11 shows the damage image obtained by a conventional immersion ultrasonic C-scan method. Compared with Fig.11, the large amount of the wave energy in the "health" area reduces the resolution of damage image in Fig.10.

After filtering the reflected wave, the AIW energy map can be obtained according to Eq. (5). Compared with calculating anomalous wave directly from the original wavefield, AIW extracts the wave propagation changes caused by the impact damage, and removes the negative influence from the reflected waves. Fig.12 shows the damage evaluation result using AIW energy map.

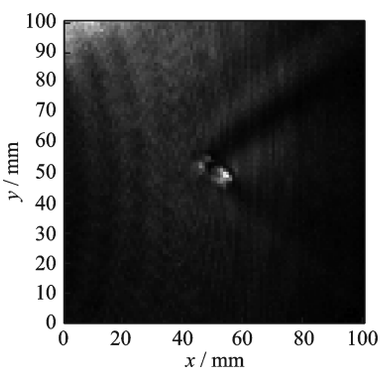

Fig.10 Damage evaluation using the original wave energy map

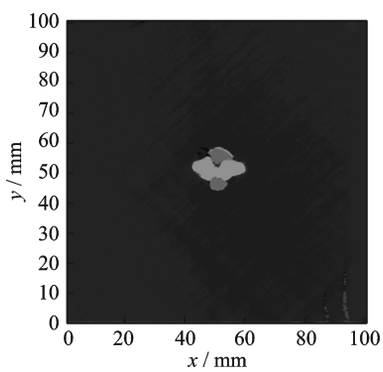

Fig.11 Damage evaluation using immersion ultrasonic C-scan method

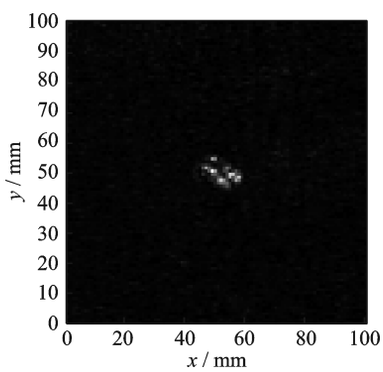

Fig.12 Damage evaluation using the AIW energy map

2 Stiffness Reconstruction

Identification of material's mechanical properties for composites is fundamental in laminate structures design, and it also provides a nondestructive approach for evaluating composite fatigue accumulated damages[37-38]. The stiffness of laminates may change due to stress or heat induced fatigue damages. Evaluating material properties of the composites periodically thus enables monitoring the health of the structures. Conventional techniques like tensile, compression and shear tests can be destructive in nature and provide only a few of the elastic moduli. Ultrasonic techniques are more advantageous over the conventional methods due to their qualification for nondestructive measurement of the elastic moduli of such materials[39-45].

Ultrasonic-based stiffness measurement methods come with two categories: the bulk wave and the Lamb wave. Using the bulk wave to measure certain stiffness parameter is well known[46-59]. however, this method is insensitive to the in-plane C_{12} and out-of-plane C_{66}. Hence only seven stiffness parameters out of nine for composite materials can be effectively reconstructed. Another limitation of the bulk wave method is that separate samples are need-

ed, whereas Lamb wave-based techniques are in situ.

Lamb wave method has also been investigated to a certain degree[51,60-62]. Jen et al.[61] investigated the inverse problem for isotropic plates but did not conduct any experimental study. Rao[62] reconstructed the elastic moduli of a unidirectional composite plate but the error is unacceptable for C_{12} and C_{66}. Vishnuvardhan et al.[51] reconstructed the nine elastic moduli of composite laminates using a single-transmitter-multiple-receiver configuration. The inversion algorithms, GAs, are used to minimize the error between the measured velocities and the calculated ones. However, the experimentally measured group velocities were considered equal to the phase velocities during the reconstruction process, in which case the inversion results might be incorrect.

At NUAA, a laser ultrasonic system is incorporated to increase the accuracy for Lamb wave velocity measurements and GAs are then applied to invert the measured velocities and conclude to the reconstructed material properties.

2.1 GAs for the inversion of phase velocities

The GA-based inverse method of reconstruction starts with a population of randomly generated candidate values for the stiffness coefficient set, each of that are then evaluated using the error function. A few of them with the lowest error function are preserved, while the others are replaced with new trials. GAs parameters are listed in Table 1. The error function to be minimized, during the inversion of the ultrasonic phase velocities, can be represented as follows

$$\mathrm{err}(C)=\frac{1}{n}\sum_{i-1}^{n}\left|\frac{v_i^{\mathrm{e}}-v_i^{\mathrm{t}}}{v_i^{\mathrm{e}}}\right| \tag{10}$$

The objective function above describes the relative error between the experimental velocity v^{e} and the theoretical ones v^{t}. When the propagation direction is specified, n denotes the number of the chosen frequencies.

Table 1 GAs parameters used in the inversion procedure

Parameter	Value
Number of generations	1 000
Population size	20
Number of elites	2
Crossover rate	0.8
Mutation rate	0.2
Crossover type	Single point

A basic knowledge that the propagation direction of phase velocity is not same as that of the group velocity in an anisotropic plate[63] as shown in Fig. 13, should be taken into account in GAs. The snapshot in Fig. 13 is based on an FEM simulation of Lamb wave propagation at a given frequency in a unidirectional plate whose properties are listed in Table 2. The direction of group velocity is along the white dot line that implies the sensing line in experiments, while the relevant phase velocity travels perpendicular to the wave front. Because the measured velocity v_e is obtained from the group angle, the relevant theoretical phase velocity, which is perpendicular to the wave front, should be transformed to the group velocity coordinate by

$$v_t=v'_t/\cos(\theta) \tag{12}$$

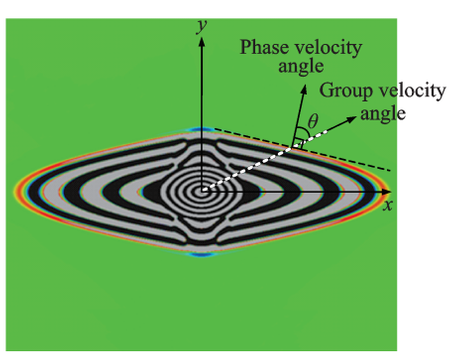

Fig. 13 Schematic of different propagation angle between phase velocity and group velocity in a unidirectional plate (based on an FEM snapshot)

Table 2 Typical stiffness coefficients[65] for two CFRP plates with thickness of 1 mm and density of 1 600 kg/m³

GPa

Parameter	C_{11}	C_{12}	C_{13}	C_{22}	C_{23}	C_{33}	C_{44}	C_{55}	C_{66}
Unidirectional	155.43	3.72	3.72	16.34	4.96	16.34	3.37	7.48	7.48
Cross-ply	77.40	6.24	5.81	73.40	5.81	12.43	4.26	4.26	5.00

where θ is the angle between the phase velocity and the group velocity.

2.1.1 Sensitivity analysis of phase velocities to the change of stiffness coefficients

In the study[64], the authors reconstructed the material properties using a series of angles from 0° to 90° (considering the symmetric characteristic of the chosen plate) with an increment of 0.2°, which increases the complexity of the inversion problem by a significant margin. To simplify the reconstruction process and improve the efficiency, a sensitivity analysis should be performed to identify regions where the change of the material properties significantly affects the measured Lamb wave velocities. In addition, the relative sensitivity of unknown parameters (elastic moduli) becomes important in a multiparameter optimization problem as described in this section. If the sensitivities of the nine parameters are remarkably different from each other, then the performance of the GAs may not be reliable, that is, the error of the reconstructed elastic moduli will be larger for some of the elastic moduli, to which the velocities are less sensitive.

To simplify the inversion procedure and improve the reliability of the reconstructed multiple parameters, a sensitivity analysis of the phase velocity to the change of the nine stiffness coefficients along 0° to 90° is conducted at a specified frequency, as illustrated in Fig. 14. The horizontal coordinate denotes the group velocity direction and the phase velocities have been transformed to the group velocity direction. The vertical coordinate denotes the relative difference of the phase velocities when each stiffness coefficient is increased by 20%.

During the sensitivity analysis, the material properties of the two plates are given in Table 2 that shows the typical stiffness coefficients of a unidirectional and a cross-ply CFRP plates. However, this does not mean that the experimental specimens are of the same material properties in Table 2.

According to Fig.14(a), for both plates, phase velocities of A_0 mode in 0° direction are most sensitive to C_{11} and C_{55}. Phase velocities of A_0 mode in 90° direction are most sensitive to C_{22} and C_{44}, while phase velocities of A_0 mode in the 20°—60° region are sensitive to C_{12} and C_{66}. However, A_0 mode velocities are much less sensitive to the left three parameters (C_{13}, C_{23}, and C_{33}) and thus A_0 mode velocities cannot be used to reconstruct the left three stiffness coefficients efficiently.

As for S_0 mode, as shown in Fig.14(b), velocities in 0° direction are more sensitive to C_{11} and C_{13},

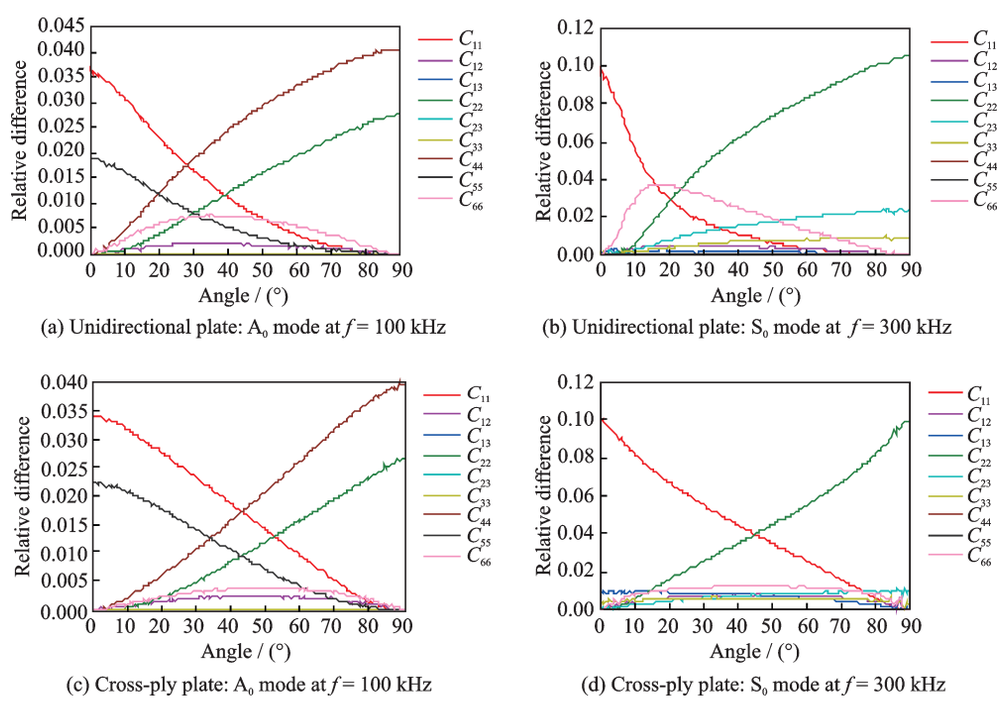

(a) Unidirectional plate: A_0 mode at f = 100 kHz

(b) Unidirectional plate: S_0 mode at f = 300 kHz

(c) Cross-ply plate: A_0 mode at f = 100 kHz

(d) Cross-ply plate: S_0 mode at f = 300 kHz

Fig.14 The relative difference of phase velocities when varying each stiffness coefficient by 20%

velocities in 90° direction are more sensitive to C_{22}, C_{23}, and C_{33}. Velocities in 20° direction are most sensitive to C_{12} and C_{66} for the unidirectional plate, while velocities in 45° direction are most sensitive to C_{12} and C_{66} for the cross-ply one.

Although both A_0 and S_0 mode velocities in 0° direction are sensitive to C_{11}, S_0 mode is chosen to reconstruct C_{11} due to its higher objective function value (higher sensitivity) compared with that of A_0 mode. Similarly, S_0 mode velocities are more sensitive to C_{22}, C_{12}, and C_{66} and will be inversed to reconstruct these three parameters.

By comparison and combination of A_0 mode and S_0 mode, the reconstructing method regarding the specific combination of modes and directions is illustrated in Tables 3, 4. The C_{11} and C_{22} using S_0 mode velocities are reconstructed first and regarded as known when inverting C_{44} and C_{55} using A_0 mode velocities. To avoid non-uniqueness of solution for the multiparameter problem, phase velocities at a serious of frequencies (dispersion curves) will be utilized in GAs.

2.1.2 Reconstruction method

The reconstruction of the nine stiffness coefficients was carried out for two different CFRP plates. With MATLAB Optimization Tool, the material properties were identified by inverting the experimental velocities shown in Fig.15. According to the reconstruction method in Tables 3, 4, C_{55} and C_{44} are taken from the reconstruction results in 0° and 90° direction of A_0 mode, respectively. C_{11} and C_{13} are identified using the S_0 mode velocities in 0° direction. Based on the S_0 mode velocities in 90° direction, C_{22}, C_{23}, and C_{33} are calculated. As shown in Fig.15(b), phase velocities in the unidirectional plate along 20° direction are sensitive not only to C_{12}

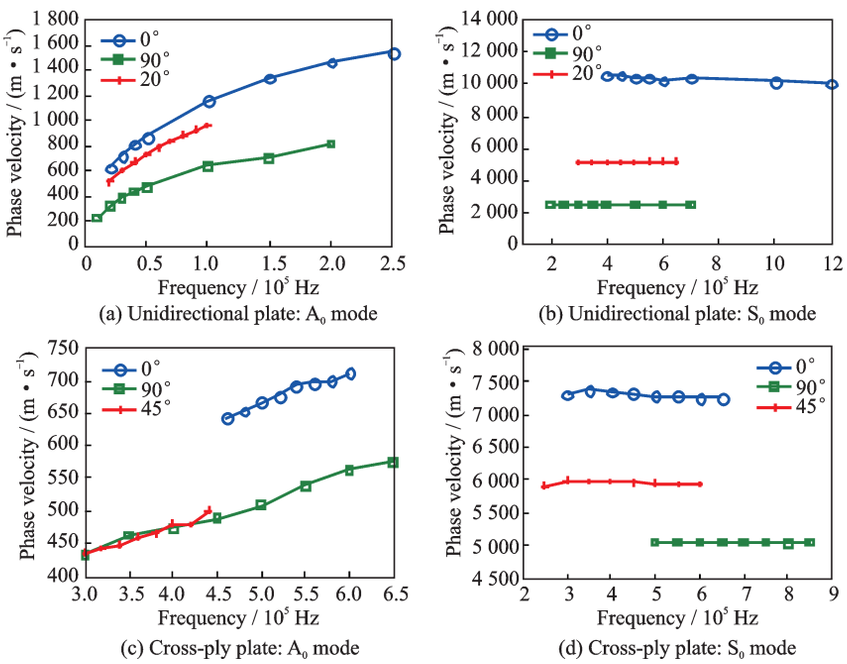

Fig.15 The experimental phase dispersion curves along specific directions

Table 3 Reconstruction method of stiffness coefficients in a unidirectional plate

Parameter to be reconstructed	C_{11}	C_{12}	C_{13}	C_{22}	C_{23}	C_{33}	C_{44}	C_{55}	C_{66}
Using Lamb wave mode	S_0	S_0	S_0	S_0	S_0	S_0	A_0	A_0	S_0
Using direction/(°)	0	20	0	90	90	90	90	0	20

Table 4 Reconstruction method of stiffness coefficients in a cross-ply plate

Parameter to be reconstructed	C_{11}	C_{12}	C_{13}	C_{22}	C_{23}	C_{33}	C_{44}	C_{55}	C_{66}
Using Lamb wave mode	S_0	S_0	S_0	S_0	S_0	S_0	A_0	A_0	S_0
Using direction/(°)	0	45	0	90	90	90	90	0	45

and C_{66} but also to others. To assure the accuracy of the reconstructed value of C_{12} and C_{66}, the other seven parameters should be identified first and substituted into GAs for the further reconstruction of C_{12} and C_{66}.

2.2 Results and discussion

2.2.1 Reconstructed results

The reconstructed results are listed in Tables 5, 6. The relative phase velocities error along 0° and 90° of S_0 mode is less than 1% and thus the reconstructed results (C_{11}, C_{13}, C_{22}, C_{23} and C_{33}) are of high accuracy according to the sensitivity analysis in Fig.14. The objective function value in 90° direction of A_0 mode is always the highest, which might result from the inaccuracy and the unsmooth dispersion curve of the experimental velocities in 90° direction of A_0 mode.

2.2.2 Verification of the reconstructed results

To verify the accuracy of the reconstructed results in Tables 5, 6, the nine parameters are substituted into a commercial software ABAQUS, as the material properties, to simulate the propagation characteristics of Lamb waves. A normal-to-plane nodal force, whose time distribution is taken from the experimental signal sensed by the AE transducer when the laser source points at the position of the sensor, as shown in Fig.3, is set as the load condition in the FEM simulation. The model is pinned at the boundaries. The element is of liner solid type and the element size is set as 0.3 mm×0.3 mm. The maximum time step of the explicit scheme is set as 0.01 μs. The simulation results are compared with the experimental images, as shown in Fig.16. The wave curves of the simulated three basic Lamb wave modes coincide well with the experimental ones.

Meanwhile, the calculated and measured velocities curves of S_0 mode are compared in Fig.17. As illustrated in Figs.17(a), (c), the theoretical and experimental dispersion curves in 0° and 90° directions of S_0 mode coincide well. There exists difference between the theoretical and experimental dis-

Table 5 Reconstructed parameters and the objective function of the unidirectional plate

Lamb wave mode and direction		Parameter	Reconstructed value/GPa	Objective function value/% (error)
A_0	0°	C_{55}	5.99	1.74
	90°	C_{44}	2.10	4.06
S_0	0°	C_{11}	175.72	0.74
		C_{13}	14.53	
	90°	C_{22}	11.76	0.34
		C_{23}	8.54	
		C_{33}	13.81	
	20°	C_{12}	10.08	2.71
		C_{66}	6.33	

Table 6 Reconstructed parameters and the objective function value of the cross-ply plate

Lamb wave mode and direction		Parameter	Reconstructed value/GPa	Objective function value/ % (error)
A_0	0°	C_{55}	1.51	0.79
	90°	C_{44}	0.58	4.88
S_0	0°	C_{11}	93.60	0.24
		C_{13}	10.10	
	90°	C_{22}	65.70	0.20
		C_{23}	11.70	
		C_{33}	16.40	
	45°	C_{12}	11.01	1.82
		C_{66}	3.99	

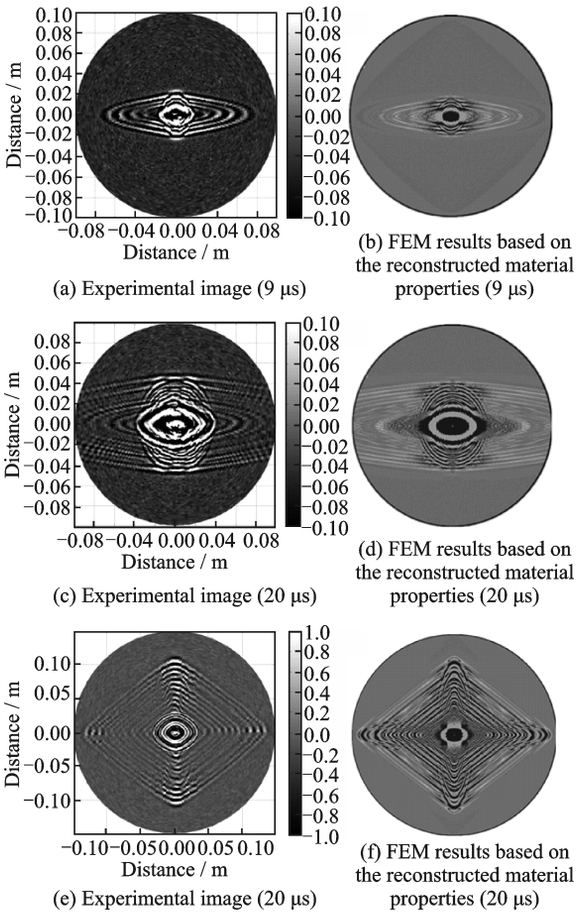

Fig.16 Comparison of the snapshots of Lamb waves propagation (Unidirectional plate: (a) — (d); Cross-ply plate: (e)—(f))

persion curves in other directions (20° for the unidirectional plate and 45° for the cross-ply one), which is mainly because that the reconstruction process of these directions is based on the 0° and 90° directions results and the previous error is brought in.

Information in only three directions is utilized in the inversion procedure and thus velocities in other directions need to be verified. For the unidirectional plate, the experimental velocities of S_0 mode (f = 500 kHz) in other seven directions (10°, 30°, 40°, 50°, 60°, 70°, and 80°) were extracted from the laser ultrasonic results and were found to agree well with the theoretical ones, as shown in Fig.17 (b). In Fig.17 (d), the measured velocities of S_0 mode (f = 500 kHz) in the cross-ply plate in other eight directions (10°, 20°, 30°, 40°, 50°, 60°, 70°, and 80°) are taken into account and also match the theoretical ones.

3 Conclusions

Laser ultrasonic technique has shown great potentials for NDT applications in composite structures. The utilization of laser ultrasonic can help to ensure the safety of composite structures and prolong the service life. It is extremely useful in the background of composite materials being widely used in various industries. This paper concludes two main applications developed at NUAA that employs laser ultrasonic technique for damage detection and

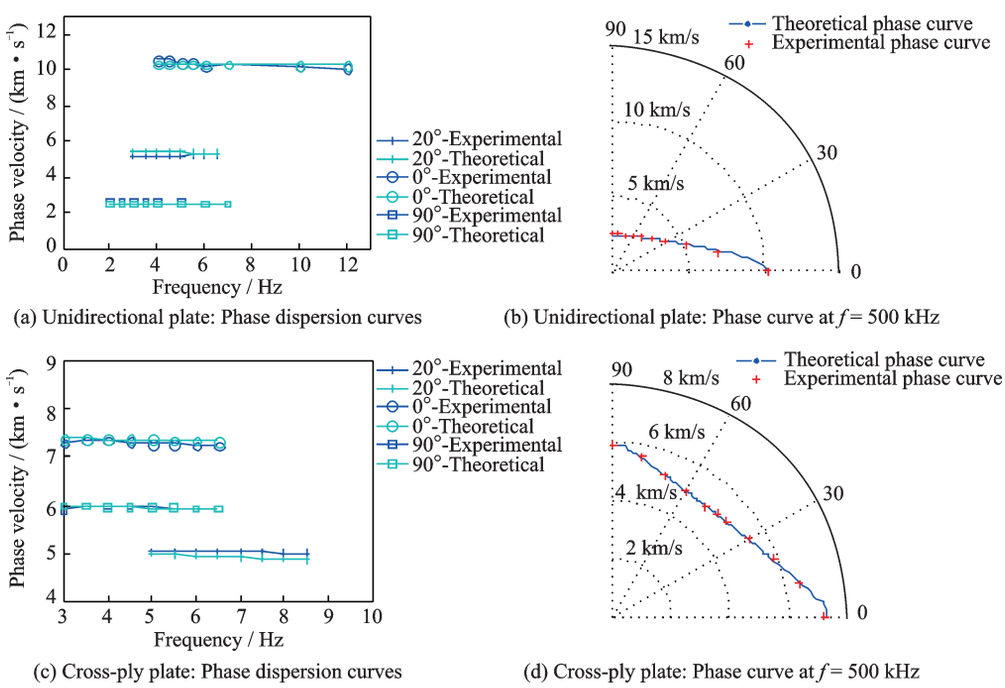

Fig.17 Comparison of the experimental and theoretical phase velocities of S_0 mode based on the reconstructed results

stiffness parameter reconstruction for composite laminates, which covers from the manufacture to various service conditions of composite laminates. For damage detection, an AIW-based damage visualization algorithm is proposed that not only captures the wave propagation changes caused by the impact damage, but also removes the negative influence from the reflected waves resulting in a much-improved resolution for damage visualization. In terms of stiffness reconstruction, a thorough sensitivity analysis has been conducted to reduce the complexity for the inverse problem, which was solved using GAs, the utilization of laser ultrasonic technique improved the accuracy for velocity extraction leading to a better reconstruction result.

Based on current foundations, ongoing research aims to develop a comprehensive and compact laser inspection system that is capable to realize in-situ, noncontact and nondestructive inspections for both normal and curved composite structures, detecting macroscopic damages e.g. impact damages, major delamination etc., as well as microscopic damages, e.g. fatigue cracks.

References

[1] BLITZ J, SIMPSON G. Ultrasonic methods of non-destructive testing[M]. Springer Science & Business Media, 1995.

[2] GIURGIUTIU V, ZAGRAI A, BAO J. Damage identification in aging aircraft structures with piezoelectric wafer active sensors[J]. Journal of Intelligent Material Systems and Structures, 2004, 15(9/10): 673-687.

[3] IHN J-B , CHANG F-K. Pitch-catch active sensing methods in structural health monitoring for aircraft structures[J]. Structural Health Monitoring, 2008, 7(1): 5-19.

[4] GIURGIUTIU V. Tuned Lamb wave excitation and detection with piezoelectric wafer active sensors for structural health monitoring[J]. Journal of Intelligent Material Systems and Structures, 2005, 16(4): 291-305.

[5] ASKAR'YAN G, PROKHOROV A, CHANTURIYA G, et al. The effects of a laser beam in a liquid [J]. Sov Phys JETP, 1963, 17(6): 1463-1465.

[6] WHITE R M. Generation of elastic waves by transient surface heating[J]. Journal of Applied Physics, 1963, 34(12): 3559-3567.

[7] DAVIES S, EDWARDS C, TAYLOR G, et al. Laser-generated ultrasound: Its properties, mechanisms and multifarious applications[J]. Journal of Physics D: Applied Physics, 1993, 26(3): 329.

[8] HUTCHINS D. Ultrasonic generation by pulsed lasers [M]. Physical Acoustics. Houand: Elsevier, 1988: 21-123.

[9] SCRUBY C B, DRAIN L E. Laser ultrasonics techniques and applications[M]. [S. l.]: CRC Press, 1990.

[10] STASZEWSKI W, LEE B, TRAYNOR R. Fatigue crack detection in metallic structures with Lamb waves and 3D laser vibrometry[J]. Measurement Science and Technology, 2007, 18(3): 727.

[11] LEE J H, LEE S J. Application of laser-generated guided wave for evaluation of corrosion in carbon steel pipe[J]. Ndt & E International, 2009, 42(3): 222-227.

[12] YASHIRO S, TAKATSUBO J, MIYAUCHI H, et al. A novel technique for visualizing ultrasonic waves in general solid media by pulsed laser scan[J]. NDT & E International, 2008, 41(2): 137-144.

[13] CHIA C C, LEE J R , SHIN H J . Hot target inspection using a welded fibre acoustic wave piezoelectric sensor and a laser-ultrasonic mirror scanner[J]. Measurement Science and Technology, 2009, 20(12): 127003.

[14] AN Y K, PARK B, SOHN H. Complete noncontact laser ultrasonic imaging for automated crack visualization in a plate[J]. Smart Materials and Structures, 2013, 22(2): 025022.

[15] FINK M, PRADA C. Acoustic time-reversal mirrors [J]. Inverse Problems17, 2001, 17:1-38.

[16] ACHENBACH J. Reciprocity in elastodynamics[M]. U.K.: Cambridge University Press, 2003.

[17] LEE J R, CHIA C C, PARK C Y, et al. Laser ultrasonic anomalous wave propagation imaging method with adjacent wave subtraction: Algorithm[J]. Optics & Laser Technology, 2012, 44(5): 1507-1515.

[18] LEE J R, CHONG S Y, SUNUWAR N, et al. Repeat scanning technology for laser ultrasonic propagation imaging[J]. Measurement Science and Technology, 2013, 24(8): 085201.

[19] QIAN Z, QIU J, ZHANG C, et al. Application of laser ultrasonic detection method for double-layer laminated material[J]. Laser & Optoelectronics Progress, 2016, 53(3): 031402.

[20] LEE J R, JEONG H, CIANG C C, et al. Applica-

tion of ultrasonic wave propagation imaging method to automatic damage visualization of nuclear power plant pipeline[J]. Nuclear Engineering and Design, 2010, 240(10): 3513-3520.

[21] DIXON S, BURROWS S E, DUTTON B, et al. Detection of cracks in metal sheets using pulsed laser generated ultrasound and EMAT detection[J]. Ultrasonics, 2011, 51(1): 7-16.

[22] LEE J R, SHIN H J, CHIA C C, et al. Long distance laser ultrasonic propagation imaging system for damage visualization[J]. Optics and Lasers in Engineering, 2011, 49(12): 1361-1371.

[23] SOHN H, DUTTA D, YANG J, et al. Automated detection of delamination and disbond from wavefield images obtained using a scanning laser vibrometer[J]. Smart Materials and Structures, 2011, 20(4): 045017.

[24] CHIA C C, JEONG H M, LEE J R, et al. Composite aircraft debonding visualization by laser ultrasonic scanning excitation and integrated piezoelectric sensing [J]. Structural Control and Health Monitoring, 2012, 19(7): 605-620.

[25] LEE H, YANG J, SOHN H. Baseline-free pipeline monitoring using optical fiber-guided laser ultrasonics [J]. Structural Health Monitoring—An International Journal, 2012, 11(6): 684-695.

[26] MARTARELLI M, CHIARIOTTI P, PEZZOLA M, et al. Delamination detection in composites by laser ultrasonics[C]//AIP Conference Proceedings. Ancona, Italy, 2014: 405-412.

[27] PARK B, AN Y K, SOHN H. Visualization of hidden delamination and debonding in composites through noncontact laser ultrasonic scanning[J]. Composites Science and Technology, 2014, 100: 10-18.

[28] SUN G K, ZHOU Z G. Application of laser ultrasonic technique for non-contact detection of drilling-induced delamination in aeronautical composite components [J]. Optik, 2014, 125(14): 3608-3611.

[29] CAVUTO A, MARTARELLI M, PANDARESE G, et al. Experimental investigation by laser ultrasonics for high speed train axle diagnostics[J]. Ultrasonics, 2015, 55: 48-57.

[30] LIU P, SOHN H, YANG S, et al. Fatigue crack localization using noncontact laser ultrasonics and state space attractors[J]. Journal of the Acoustical Society of America, 2015, 138(2): 890-898.

[31] BATE P, LUNDIN P, LINDH-ULMGREN E, et al. Application of laser-ultrasonics to texture measurements in metal processing[J]. Acta Materialia, 2017, 123: 329-336.

[32] ZHANG C, QIU J, JI H. Laser ultrasonic imaging for impact damage visualization in composite structure [C]. EWSHM—7th European Workshop on Structural Health Monitoring Nantes, France: Hal-Inria, 2014.

[33] CHIA C C, LEE J R, PARK C Y, et al. Laser ultrasonic anomalous wave propagation imaging method with adjacent wave subtraction: Application to actual damages in composite wing[J]. Optics & Laser Technology, 2012, 44(2): 428-440.

[34] RUZZENE M. Frequency-wavenumber domain filtering for improved damage visualization[J]. Smart Materials and Structures, 2007, 16(6): 2116.

[35] MICHAELS T E, MICHAELS J E, RUZZENE M. Frequency-wavenumber domain analysis of guided wavefields[J]. Ultrasonics, 2011, 51(4): 452-466.

[36] Standard A. D7136/D7136M-05, Standard test method for measuring the damage resistance of a fiber-reinforced polymer matrix composite to a drop-weight impact event[S]. West Conshohocken (PA): ASTM International, 2005.

[37] TAO C C, QIU J. A Lamb wave velocity degradation model for cross-ply laminates under fatigue loading [C]//AIP Conference Proceedings Atlanta, USA: AIP Conference, 2017: 090003.

[38] TAO C C, JI H L, QIU J H, et al. Characterization of fatigue damages in composite laminates using Lamb wave velocity and prediction of residual life[J]. Composite Structures, 2017, 166: 219-228.

[39] ROSE J L. Ultrasonic waves in solid media[M]. UK: Cambridge University Press, ASA, 2000.

[40] NAYFEH A H. Wave propagation in layered anisotropic media: With application to composites[M]. Holland: Elsevier, 1995.

[41] KLINE R. Nondestructive characterization of composite media[M]. U.K.: Routledge, 2017.

[42] JONES R M. Mechanics of composite materials[M]. CRC press, 2014.

[43] LIU G R, XI Z. Elastic waves in anisotropic laminates [M]. [S.l.]: CRC press, 2001.

[44] ZHAO J L, QIU J H, JI H L. Reconstruction of the nine stiffness coefficients of composites using a laser generation based imaging method[J]. Composites Science and Technology, 2016, 126: 27-34.

[45] ZHAO J, QIU J H, JI H L. Ultrasonic techniques based inversion of elastic properties for a single lamina in composites laminates[C]//8th European Workshop on Structural Health Monitoring. Bilbao, Spain:[s.n.], 2016.

[46] CHU Y, DEGTYAR A, ROKHLIN S. On determination of orthotropic material moduli from ultrasonic velocity data in nonsymmetry planes[J]. The Journal of the Acoustical Society of America, 1994, 95(6): 3191-3203.

[47] CHU Y, ROKHLIN S. Stability of determination of composite moduli from velocity data in planes of symmetry for weak and strong anisotropies[J]. The Journal of the Acoustical Society of America, 1994, 95(1): 213-225.

[48] ROKHLIN S, WANG W. Double through-transmission bulk wave method for ultrasonic phase velocity measurement and determination of elastic constants of composite materials[J]. The Journal of the Acoustical Society of America, 1992, 91(6): 3303-3312.

[49] BALASUBRAMANIAM K, RAO N S. Inversion of composite material elastic constants from ultrasonic bulk wave phase velocity data using genetic algorithms [J]. Composites Part B: Engineering, 1998, 29(2): 171-180.

[50] REDDY S S S, BALASUBRAMANIAM K, KRISHNAMURTHY C, et al. Ultrasonic goniometry immersion techniques for the measurement of elastic moduli[J]. Composite Structures, 2005, 67(1): 3-17.

[51] VISHNUVARDHAN J, KRISHNAMURTHY C, BALASUBRAMANIAM K. Genetic algorithm reconstruction of orthotropic composite plate elastic constants from a single non-symmetric plane ultrasonic velocity data [J]. Composites Part B: Engineering, 2007, 38(2): 216-227.

[52] CHIROIU C, MUNTEANU L, CHIROIU V, et al. A genetic algorithm for determination of the elastic constants of a monoclinic crystal[J]. Inverse Problems, 2000, 16(1): 121.

[53] TEIXEIRA SILVA M F, ALVES BORGES L M S, ROCHINHA F A, et al. A genetic algorithm applied to composite elastic parameters identification[J]. Inverse Problems in Science and Engineering, 2004, 12(1): 17/28.

[54] LIU G, HAN X, LAM K. A combined genetic algorithm and nonlinear least squares method for material characterization using elastic waves [J]. Computer methods in applied mechanics and Engineering, 2002, 191(17-18): 1909-1921.

[55] CASTAGNEDE B, KIM K Y, SACHSE W, et al. Determination of the elastic constants of anisotropic materials using laser-generated ultrasonic signals[J]. Journal of Applied Physics, 1991, 70(1): 150-157.

[56] REVERDY F, AUDOIN B. Elastic constants determination of anisotropic materials from phase velocities of acoustic waves generated and detected by lasers[J]. The Journal of the Acoustical Society of America, 2001, 109(5): 1965-1972.

[57] AUSSEL J D , MONCHALIN J P . Precision laser-ultrasonic velocity measurement and elastic constant determination[J]. Ultrasonics, 1989, 27(3): 165-177.

[58] ARISTÉGUI C, BASTE S. Optimal recovery of the elasticity tensor of general anisotropic materials from ultrasonic velocity data[J]. The Journal of the Acoustical Society of America, 1997, 101(2): 813-833.

[59] LEYMARIE N, ARISTÉGUI C, AUDOIN B, et al. Identification of complex stiffness tensor from waveform reconstruction[J]. The Journal of the Acoustical Society of America, 2002, 111(3): 1232-1244.

[60] KARIM M R, MAL A, BAR-COHEN Y. Inversion of leaky Lamb wave data by simplex algorithm [J]. The Journal of the Acoustical Society of America, 1990, 88(1): 482-491.

[61] JEN C, BUSSIERE J, FARNELL G, et al. Elastic constants evaluation using the dispersive property of acoustic waves[M]. [S.l.]: Plenum Press, 1984: 889-900.

[62] ROGERS W. Elastic property measurement using Rayleigh-Lamb waves[J]. Research in Nondestructive Evaluation, 1995, 6(4): 185-208.

[63] LOWE M, NEAU G, DESCHAMPS M. Properties of guided waves in composite plates, and implications for NDE[C]//AIP Conference Proceedings. [S.l.]: [s.n.], 2004: 214-221.

[64] VISHNUVARDHAN J, KRISHNAMURTHY C, BALASUBRAMANIAM K. Genetic algorithm based reconstruction of the elastic moduli of orthotropic plates using an ultrasonic guided wave single-transmitter-multiple-receiver SHM array[J]. Smart Materials and Structures, 2007, 16(5): 1639.

Acknowledgements This work was partially supported by the National Natural Science Foundation of China (Nos. 51875277, 51805261) and the State Key Laboratory of Mechanics and Control of Mechanical Structures (Nanjing University of Aeronautics and astronautics) (No. MCMS-I-0518K01).

Authors Prof. **QIU Jinhao** is currently a professor at the college of aerospace engineering, Nanjing University of Aeronautics and Astronautics. He is the leader of the program for Changjiang Scholars and Innovative Research Team in University and one of the National Scholar of Thousand-man Project. In 2014, he was elected as ASME fellow.

His research interests include smart materials, structures and their applications in aeronautical engineering and mechanical engineering.

Dr. **TAO Chongcong** is currently a lecture in engineering mechanics at Nanjing University of Aeronautics and Astronautics. He received the B.S. degree in engineering mechanics from Northwestern Polytechnical University in 2012, and the Ph.D. degree in engineering mechanics from Nanjing University of Aeronautics and Astronautics in 2018. His research interests include damage analysis, damage modelling and NDT applications for composite materials.

Prof. **JI Hongli** is currently a professor at Nanjing University of Aeronautics and Astronautics. She received the B.S. degree in mechanical engineering from Taiyuan University of Science & Technology in 2004, M.S. degree in mechanical engineering and Ph.D. degree in aerospace engineering from Nanjing University of Aeronautics and Astronautics in 2007 and 2012 respectively. From 2014 to 2016 she was a postdoctoral fellow at the Hong Kong Polytechnic University. Her main research interest is smart materials and structural systems, including SHM, NDT, vibration and noise control, etc.

Dr. **ZHANG Chao** is a lecturer at the State Key Laboratory of Mechanics and Control of Mechanical Structures, Nanjing University of Aeronautics and Astronautics. He served as research assistant in Department of Mechanical Engineering, Hong Kong Polytechnic University in 2014 and received the Ph. D. degree in Instrument Science and Technology in 2016 from NUAA. His main research interests are in non-destructive testing and structural health monitoring, especially laser ultrasonic technique, guided wave and vibration-based damage detection methods.

Dr. **ZHAO Jinling** is a lecturer from Nanjing Tech University of China. She is mainly engaged in ultrasonic non-destructive testing of composites with 6 published SCI papers, 11 EI papers, and 1 book. At present, her main research topics include stacking sequence identification, material properties reconstruction, life prediction, damage detection in complex pipelines, linear/nonlinear ultrasonic propagation theory, laser ultrasonic technology.

Author contributions Prof. **QIU Jinhao** designed the study. Dr. **TAO Chongcong** wrote the manuscript. Prof. **JI Hongli** contributed to the discussion and background of the study. Dr. **ZHANG Chao** contributed data for the damage detection part. Dr. **ZHAO Jinling** contributed data for the stiffness reconstruction part. All authors commented on the manuscript draft and approved the submission.

Competing interests The authors declare no competing interests.

(Production Editor: Zhang Tong)